High Performance Two-Arm Antenna for Super Wideband Operation

Eman G. Ouf[1], May A. El-Hassan[1], Asmaa E. Farahat[1, *],
Khalid F. A. Hussein[1], and Shaimaa A. Mohassieb[2]

Abstract—A super wideband antenna is proposed to operate in the frequency band 2.2–22 GHz. The antenna has two planar arms printed on the opposite faces of a three-layer dielectric substrate. Each arm of the antenna is capacitively coupled to a circular ring near its end to increase the impedance matching bandwidth. The dielectric substrate is customized to fit the shape of the antenna arms and the parasitic elements to reduce the dielectric loss. The substrate material is composed of three layers. The upper and lower layers are Rogers RO3003™ of 0.13 mm thickness, and the middle layer is made of paper of 2.3 dielectric constant and 2.7 mm thickness. The antenna is fed through a wide band impedance matching balun of a novel simple design. A prototype of the proposed antenna is fabricated to validate the simulation results. The experimental measurements are in good agreement with the simulation results, and both of them show that the antenna operates efficiently over the frequency band 2.2–22 GHz with minimum radiation efficiency of 97% and maximum gain of 5.2 dBi. The antenna has a bandwidth to dimension ratio (BDR) of 1755.

1. INTRODUCTION

Compact and low-profile antennas are vital in many applications such as wireless communication, high-performance aircraft, spacecraft, satellite, and missile applications [1–3]. The range of frequencies 3.1–10.6 GHz has been allocated for unlicensed ultra-wideband (UWB) by the Federal Communications Commission (FCC) [1]. UWB antennas have ratio bandwidth (RBW) of 3.4 : 1 but, unfortunately, not suitable for long-range mobile communications due to their slow adaptation rate, low transmitted power, and long signal acquisition time [1, 2]. A super wideband (SWB) antenna might be a good candidate to meet the future generations of mobile communication system requirements and are able to overcome the shortage of the UWB antennas. Moreover, the SWB technology provides higher channel capacity and improved time accuracy than the UWB technology [4, 5]. The SWB operation does not have specific operating frequency range unlike UWB. The antennas with a minimum bandwidth ratio of 10 : 1 for impedance matching are considered as SWB antennas. Various applications with varying operational frequency bands can be covered with a single SWB antenna that is functional for both short-range and long-range communications [1–5]. The challenge faced by SWB antenna designers is to reduce the antenna size without reducing the bandwidth or disturbing the radiation pattern stability. In the following, some recently published research papers concerned with the design and investigation of SWB antennas of planar structure are presented.

The work of [3] presents an SWB antenna fed through a coplanar waveguide (CPW) and composed of a modified bowtie-shaped patch and two asymmetrical ground planes printed on an FR4 substrate to achieve a frequency band of 3.03–17.39 GHz. In [6], a compact and high gain SWB antenna with operation band 5.7–40 GHz is introduced. The antenna has a basic circular patch with partial ground and a copper reflector to realize gain and bandwidth enhancement. The work of [7] presents a small bulb-shaped planar SWB antenna operating over the frequency band 2.8–40 GHz using frequency selective

surface. A compact concentric structured monopole patch antenna emerging from a traditional circular monopole antenna for SWB microwave application in the range 1.2–47 GHz is proposed and investigated in [8]. In [9], a circular-hexagonal fractal antenna with a circular metallic patch and a transmission line with partial ground plane are used for designing an SWB antenna to achieve a frequency band ranging from 2.18 GHz to 44.5 GHz. The work of [10] proposes an SWB monopole antenna consisting of an octagonal-ring shaped patch. Both the patch and feed line are shifted off the center line with a notch made in the ground plane to get the antenna operational over the frequency band 2.59–31.14 GHz.

This paper introduces an SWB antenna design with matched impedance between 2.2 and 22 GHz. The antenna is constructed as a dipole with diamond shape arms with blended corners, capacitively coupled to annular ring elements for wide band impedance matching. The substrate has customized size to fit the conducting metal surface of the antenna and composed of three layers to implement a gradient profile of the dielectric constant for improving the impedance matching bandwidth. A wide band feeding balun is employed to feed the proposed two balanced arms of the antenna using the unbalanced coaxial line.

The present paper is organized as follows. Section 2 introduces the design of the antenna. Section 3 presents the antenna fabrication and measurements of the return loss compared to simulation. Section 4 describes the process of measuring the gain and radiation patterns, and provides comparison with the simulation results. Section 5 demonstrates the simulated and measured gains and radiation efficiencies with the frequency. Section 6 gives some comparisons between the performance of the antenna proposed in the present work and other SWB antennas presented in recently published work. Finally, Section 7 summarizes the conclusions of the present work.

2. DESIGN OF THE PROPOSED ANTENNA

A new design for an SWB antenna is proposed in this work. The antenna is constructed as an antenna with two diamond arms fed through a balun with a novel structure. The radiating antenna and the balun used for feeding the antenna are explained in the following sections.

2.1. Design of the Radiating Arms of the Antenna

The design of the proposed SWB antenna is shown in Figures 1 and 2. The antenna is constructed as a dipole of two diamond shape arms with blended corners, capacitively coupled to two annular rings through a narrow circular gap to increase the impedance matching bandwidth.
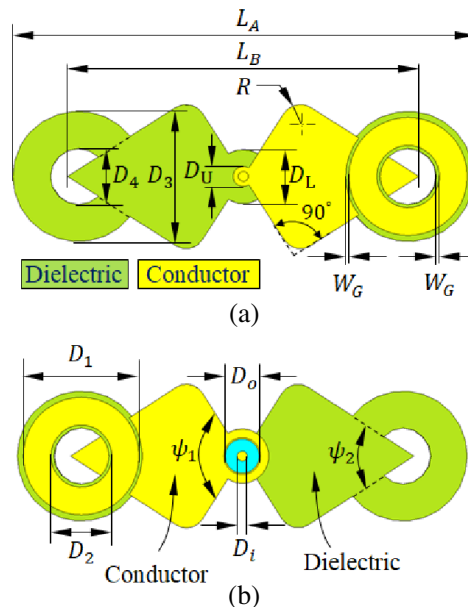

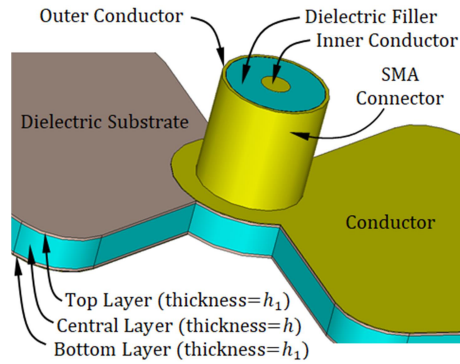**Figure 1.** (a) Upper, and (b) lower, surface of the proposed SWB antenna.

Figure 2. Substrate structure and the coaxial feeder connected to the antenna through the balun.

The angular extension of each arm in any two-arm antenna helps to increase the operational bandwidth. However, the limited length of the antenna arms limits both the lower and higher frequencies of the operational band. Therefore, placing the capacitively coupled elements of the appropriate shape and dimensions near the end of each arm has the effect of adapting the antenna impedance by effectively adding a reactive load to the original antenna arms. Thus, the total impedance seen at the antenna feeding port can be adjusted by setting the dimensions of the reactively coupled loads so as to reduce the imaginary part of the impedance and to get the real part as close as possible to $50\,\Omega$. The mission of the antenna designer, in this case, is to arrive at the appropriate shape, dimensions, and placement of the capacitively coupled elements to realize the required bandwidth for impedance matching.

The geometry of the upper and lower surfaces of the proposed antenna is shown in Figure 1. The substrate is composed of three layers. The upper and lower layers are Rogers RO3003$^{\text{TM}}$ with $\varepsilon_{r1} = 3$ and height $h_1 = 0.13\,\text{mm}$. The middle layer is made of quality paper with $\varepsilon_{r2} = 2.3$ and height $h_2 = 2.7\,\text{mm}$. The substrate is cut with the same size and shape of the metallic conducting surface of the antenna arms. One arm is printed on the upper surface of the substrate and the other arm printed on the lower surface on the other side of the substrate as shown in Figure 1. The antenna is fed through a coaxial feeder using a wideband impedance matching balun. The balun structure is explained in the next section.

The super wideband characteristics of the antenna and its high efficiency are attributed to: (i) The wide angle ψ_1 of the tapered shape arm that increases the bandwidth. (ii) Increasing the bandwidth through smoothing of the sharp corners of the diamond shape arms. (iii) The capacitive coupling of the arms of the antenna with annular sector shape parasitic elements improves the antenna matching and, hence, increases the bandwidth. (iv) Cutting the substrate material on the shape of the metallic surfaces instead of using conventional rectangular substrate to reduce the dielectric losses. (v) Constructing the substrate with multilayer dielectric with different dielectric constants with certain profile reduces the dielectric losses and, hence, increases the radiation efficiency. (vi) Feeding the antenna using wideband balun increases the input impedance matching bandwidth. This balun is constructed from two circular discs with radii D_L and D_U, lower and upper diameters, respectively. The lower disc is connected to the outer conductor of the coaxial feed line as shown in Figure 2 and the upper disc connected to the inner conductor of the feed line as shown in Figure 1(a). The radii of the upper and lower discs and the distance between them, L_P, control the operating band.

The optimum dimensions of the proposed antenna shown in Figure 1 are presented in Table 1. These parameters are obtained through extensive electromagnetic simulations. Parametric studies are investigated for some effective parameters of the design.

Table 1. Optimum parameters of the SWB antenna design shown in Figure 1.

Parameter	L_A	L_B	D_1	D_2	D_3	D_4	D_L	D_U	D_i	D_o	W_G	h	h_1	R	ψ_1	ψ_2
Value (mm)	71.8	60	15.2	8	16.8	7.2	5.6	2.4	1.3	4.45	0.4	2.7	0.13	2	126°	54°

2.2. Design of the Feeding Balun

The balun design introduced in this work is constructed from annular discs separated by a distance, L_P, which is specified by the substrate height. The lower disc is soldered to the outer conductor of the coaxial feed line, and the upper disc is soldered to the inner conductor of the coaxial feed line. The proposed balun design connected to the coaxial feed is illustrated in Figure 3. D_L and D_U are the diameters of the lower and upper annular discs of the balun, respectively, whereas D_i and D_o are the inner and outer diameters of the coaxial feed line, respectively. This balun feeds the proposed antenna in the same way as a probe feeding a microstrip patch, where inner conductor of the probe extends to the patch upper surface, and the outer conductor of the probe is connected to the GND plane of the patch. The operating bandwidth of the antenna is adjusted through the two diameters D_L and D_U, and the length L_P.
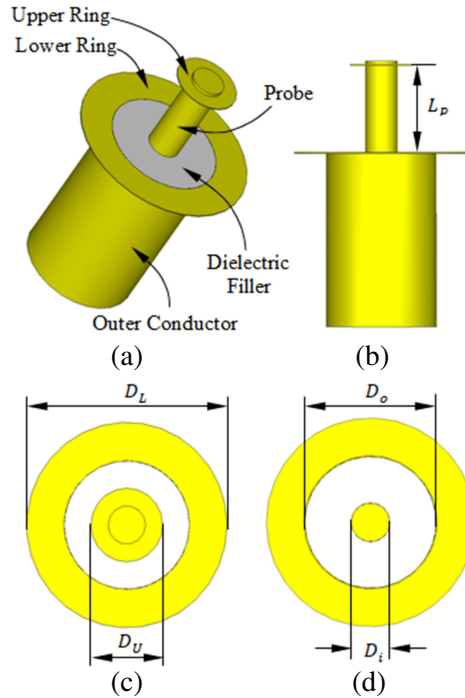

Figure 3. Feeding balun of the proposed antenna. (a) Three dimensional. (b) Lateral. (c) Top. (d) Bottom, view.

3. SIMULATION AND MEASUREMENT RESULTS

The proposed antenna is fabricated, and experimental measurements are performed and compared to the simulation results in this section.

3.1. Antenna Optimum Design Parameters Selection through Electromagnetic Simulations

The radiating elements of the proposed antenna are the diamond shaped arms and the ring-shaped parasitic elements. This subsection is concerned with the presentation and discussion of some examples of parametric studies to get the best values of the most important dimensional parameters including rhombic dipole length L_B and flare angle ψ_1.

The modified diamond shape dipole length, L_B, strongly affects the operating band of the antenna. The reflection coefficient, $|S_{11}|$, is calculated numerically for different values of L_B. The results are shown in Figure 4 and found to have the best value (wider operating bandwidth) at $L_B = 6$ cm.
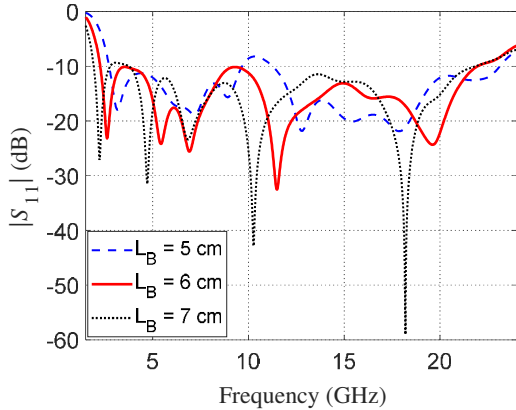
Figure 4. Calculated Reflection coefficient $|S_{11}|$ with frequency for different values of the dipole arm length, L_B.
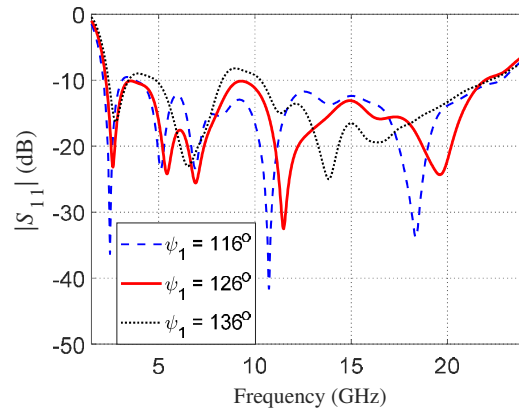

Figure 5. Calculated Reflection coefficient $|S_{11}|$ with frequency for different values of the flare angle ψ_1.

The flare angle ψ_1 can also dramatically affect the operating band of the antenna. The optimum value for this angle is obtained when $\psi_1 = 126°$. Figure 5 shows the simulated reflection coefficient for different values of the flare angle when $\psi_1 = 116°$, $126°$, and $136°$.

3.2. Optimum Balun Design Parameters

The proposed balun explained in Section 2.2 plays the main role of the antenna impedance matching over the SWB (2.2–22 GHz). This subsection is concerned with finding the best values of the three balun parameters, L_P (or equivalently the substrate height h), lower circular disc diameter D_L, and the upper circular disc diameter, D_U, to realize the required impedance matching.

The effects of the diameter of the lower and upper annular discs of the balun, D_L and D_U, on the reflection coefficient $|S_{11}|$ response over the frequency are presented in Figures 6 and 7, respectively. It is shown that the values of $D_L = 5.6$ mm and $D_U = 2.4$ mm result in the wider operating band (2.2–22 GHz).

The effect of the distance between the upper and lower annular discs of the balun L_P, which is also the substrate height, on the reflection coefficient of the antenna is studied numerically using the CST® simulator. The results are shown in Figure 8. The best value for L_P is found to be 2.7 mm which results in the wider impedance matching over the required operating frequency band (2.2–22 GHz).
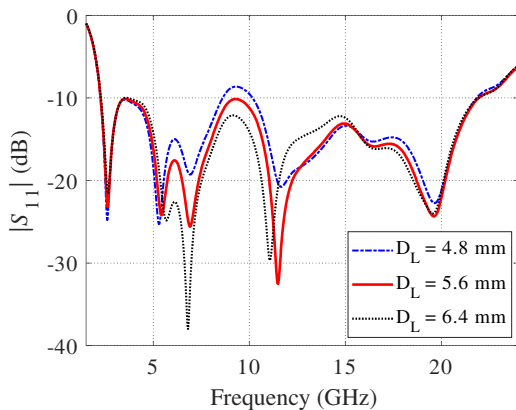

Figure 6. Calculated Reflection coefficient $|S_{11}|$ with frequency for different values of the diameter of the lower annular disc of the balun, D_L.
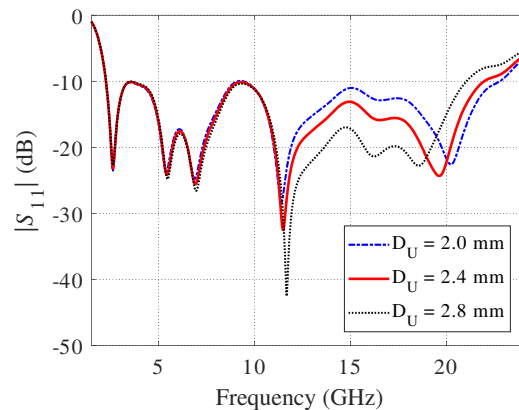

Figure 7. Calculated Reflection coefficient $|S_{11}|$ with frequency for different values of the diameter of the upper annular disc of the balun, D_U.
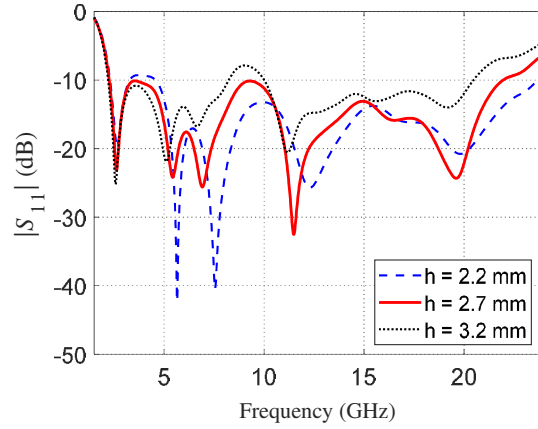
Figure 8. Calculated Reflection coefficient $|S_{11}|$ with frequency with varying the distance between the two balun discs, L_P or equivalently, substrate height, h.

3.3. Surface Current Distribution and Radiation Mechanism

The surface current distribution is calculated numerically at different frequencies. At the start frequency of the impedance matching band at 2 GHz, the surface current distribution is shown in Figure 9(a). It
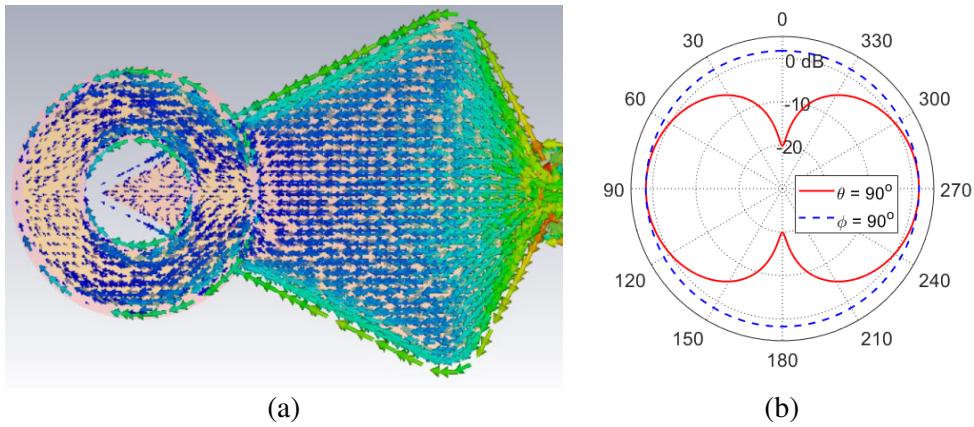

(a)   (b)

Figure 9. (a) Surface current distribution. (b) Radiation pattern, at 2 GHz.

(a)   (b)
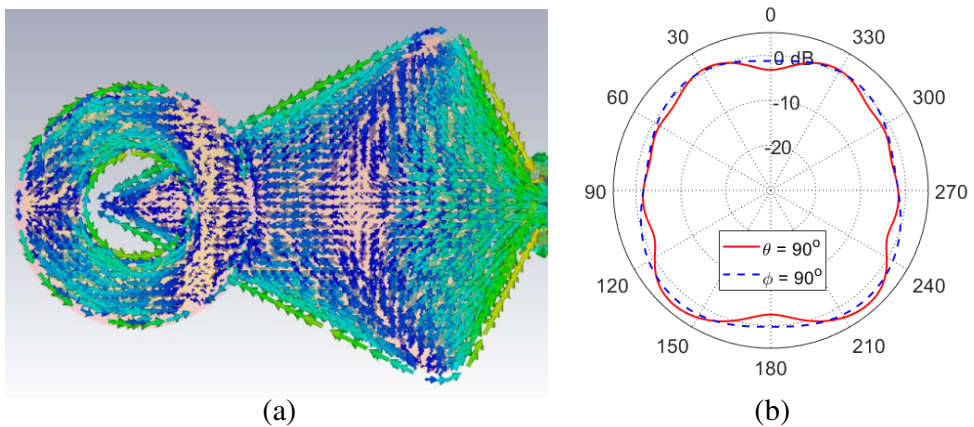
Figure 10. (a) Surface current distribution. (b) Radiation pattern, at 10 GHz.

can be seen that the effective area that has significant current magnitude is the area near the feeding on the diamond shape arm. This results in the radiation pattern shown in Figure 9(b).

Near the center frequency of the operating band at 10 GHz, the surface current distribution is investigated in Figure 10(a). As can be seen from the figure, the current vanishes at the arm center which indicates a second order mode. Also, a significant current is present on the circular ring. At this frequency, the main arm and circular ring parasitic element contribute to the far-field radiation. The radiation from parasitic element has compensated the nulls in the radiation pattern resulting in the near isotropic pattern shown in Figure 10(b).

At 22 GHz, the surface current has a higher order mode which can be seen from the distribution presented in Figure 11(a). The presence of higher order mode results in a radiation pattern with nulls at 22 GHz. The radiation pattern is shown in Figure 11(b).
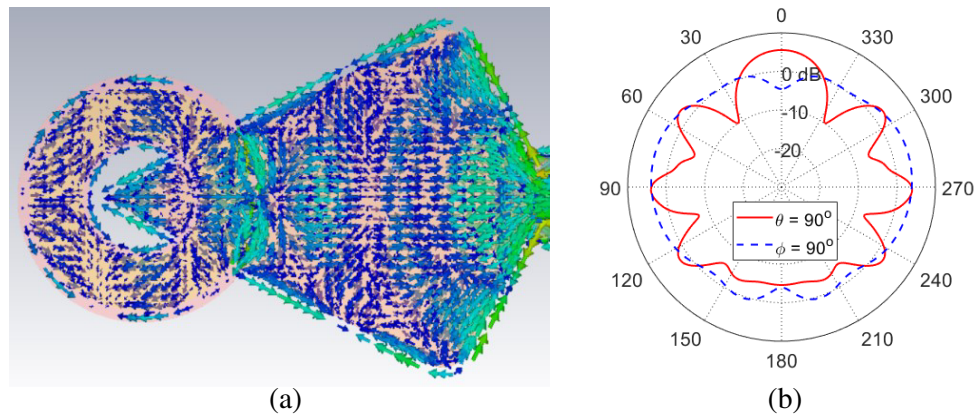

(a)   (b)

Figure 11. (a) Surface current distribution. (b) Radiation pattern, at 22 GHz.

3.4. Fabrication and Measurements of the Final Design

After performing the electromagnetic simulations and obtaining the best values for the antenna design parameters given in Table 1, a prototype is fabricated for the experimental verifications and measurements. The experimental results are compared to those obtained by the electromagnetic simulation using the CST® simulator regarding the reflection coefficient, radiation pattern, gain, and radiation efficiency. The top and bottom views of the proposed antenna are shown in Figures 12(a) and 12(b), respectively. Images of the fabricated prototype are presented in Figures 12(c) and 12(d)
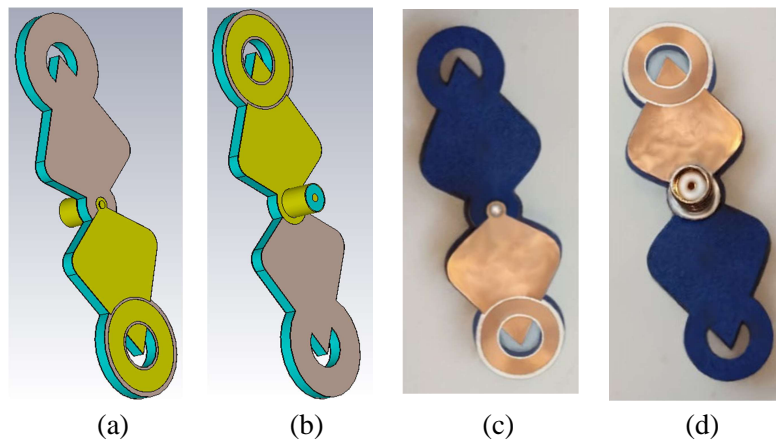

(a)   (b)   (c)   (d)

Figure 12. Three dimensional view of the (a) upper, and (b) lower isometry of the antenna. Fabricated antenna (c) top, and (d) bottom.

showing the SMA coaxial connector when being welded at the antenna input. The inner conductor is welded with the upper annular disc of the balun, and the outer conductor is soldered to the lower disc of the balun.

The vector network analyser (VNA) model Keysight N9918A is used to measure the reflection coefficient at the antenna input port. First, the VNA is calibrated using the calibration kit keysight 85521A. The antenna is then connected to the VNA using a semi-rigid coaxial cable to connect the SMA connector of the antenna to the VNA input port, as shown in Figure 13. The measured and simulated reflection coefficients S_{11} versus frequency are plotted in Figure 14 showing good agreement. As can be seen in Figure 14, the operating band below $-10\,\mathrm{dB}$ extends from about $2.2\,\mathrm{GHz}$ to $22\,\mathrm{GHz}$ for both the simulated and the measured return losses.

Figure 13. The connection of the fabricated antenna prototype to the VNA N9918A for measuring the reflection coefficient over the operating frequency band.
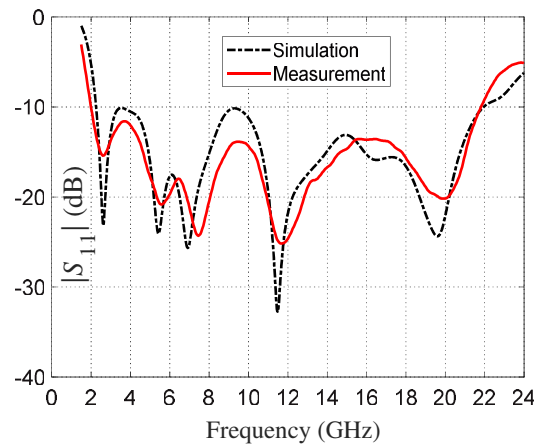

Figure 14. Measured and simulated reflection coefficient for the the designed and fabricated SWB antenna.

4. RADIATION PATTERNS

In this section, the far-field patterns of the proposed antenna are calculated and measured experimentally in the two principal planes $\phi = 0°$ and $\theta = 90°$. In Figures 15 and 16, the radiation patterns in the plane of the antenna ($\theta = 90°$) and in the plane perpendicular to the antenna ($\phi = 0°$), respectively, are calculated numerically using the CST electromagnetic simulator at different frequencies within the operating band.

Radiation pattern measurement setup is established for this purpose. Some reference-gain horn antennas are used for gain measurement of the entire frequency band of operation (2.2–22 GHz). During measurement, the reference antenna is maintained oriented to the antenna under test (AUT) which is placed on the rotator for complete rotation in the azimuth and elevation planes. The reference antenna is connected to port 1 of the VNA whereas the AUT is connected to port 2. While the AUT is rotated in the desired plane, the readings of the transmission scattering parameter S_{21} are uniformly acquired over the entire frequency band (2.2–22 GHz) with the preset resolution. A Matlab® program on the laptop plays the role of a central controller and data processor. It controls the rotation of the AUT and the data acquisition of the VNA and stores the S_{21} data during measurement. When the antenna rotation is completed, the stored S_{21} data is processed; the gain is calculated; and the radiation patterns at all the frequencies can be drawn. For example, the measured radiation patterns in the plane $\phi = 0°$ and in the plane $\theta = 90°$ at $12\,\mathrm{GHz}$ are presented in Figures 17 and 18 and compared to the radiation patterns obtained by simulation showing good agreement.
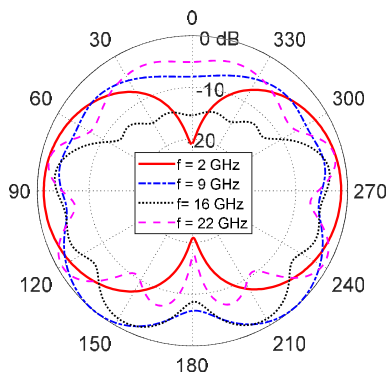
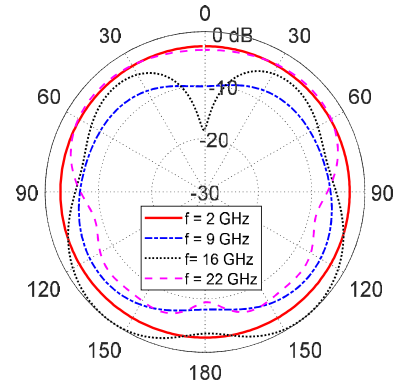**Figure 15.** Simulated far-field pattern of the SWB antenna in the plane $\theta = 90°$.

Figure 16. Simulated far-field pattern of the SWB antenna in the plane $\phi = 0°$.

Figure 17. Radiation pattern obtained by simulation and measurement for the proposed antenna, at the central frequency (12 GHz) in the plane $\theta = 90°$.

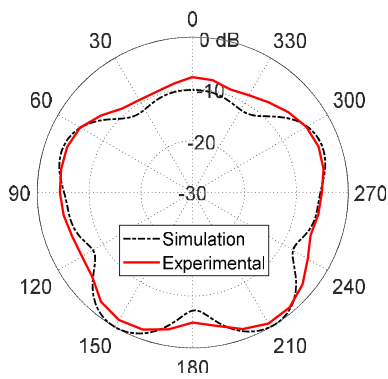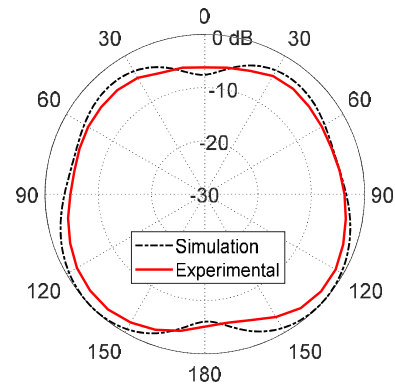**Figure 18.** Radiation pattern obtained by simulation and measurement for the proposed antenna, at the central frequency (12 GHz) in the plane $\phi = 0°$.

5. GAIN AND RADIATION EFFICIENCY OF THE PROPOSED ANTENNA

The gain and radiation efficiency of the proposed antenna are investigated by both electromagnetic simulation and experimental measurement over the frequency band (2.2–22 GHz). Figure 19 presents the variation of the maximum gain with the frequency over the entire frequency band. The dependence

Table 2. Comparison of the proposed SWB antenna with similar work.

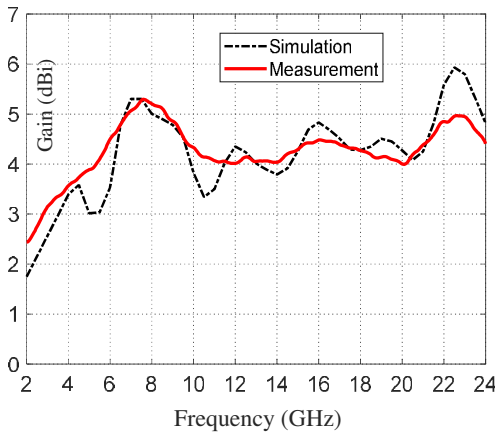| Work	Dimensions (mm × mm)	Frequency Range (GHz)	% BW	RBW	BDR	Radiation Efficiency at Start-End Frequencies
[3]	25.0×20.0	3.04–17.39	140.6%	5.7 : 1	2736	50–73%
[7]	35.0×30.0	2.8–40	173%	14 : 1	1900	60–70%
[11]	28.0×19.0	0.7–18.5	185%	26 : 1	6401	70–80%
[12]	35.0×35.0	2.3–34.8	175%	15 : 1	2433	96–52%
[Present]	71.8×24.2	2.2–22.0	164%	10 : 1	1755	99–97.5%

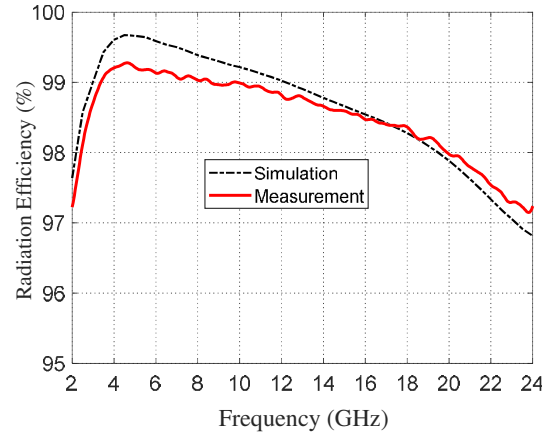**Figure 19.** Simulated and measured maximum gain with frequency of the SWB antenna shown in Figure 1.

Figure 20. Simulated and measured radiation efficiency with frequency of the SWB antenna shown in Figure 1.

of the radiation efficiency on the frequency is presented in Figure 20. It is shown that the antenna has excellent radiation efficiency over the complete frequency band. For the whole frequency range (2.2–22 GHz), the radiation efficiency is higher than 96%. The measured gain and radiation efficiency are compared to the corresponding simulation results showing good agreement.

6. COMPARISON WITH OTHER PUBLISHED WORK

The proposed antenna is compared with similar antennas in other published papers regarding the dimensions, operating bandwidth, bandwidth ratio (BW), bandwidth dimension ratio (BDR), and the antenna efficiency. The comparison is given in Table 2.

7. CONCLUSION

A super wide band antenna is proposed and printed over a customized size substrate to minimize the dielectric losses. The antenna is constructed as a dipole with modified diamond shape arms loaded with capacitive coupled parasitic element. The substrate material is composed of three layers. The upper and lower layers are Rogers RO3003$^{\text{TM}}$ of 0.13 mm thickness, and the middle layer is paper with dielectric constant of 2.3 and 2.7 mm thickness. A prototype for the proposed antenna is fabricated to validate the simulation results. Good agreement between the experimental measurements and simulations is shown regarding the reflection coefficient and radiation pattern. The antenna has operating band ranges from 2.2 GHz to 22 GHz with bandwidth to dimension ratio (BDR) of 1755 and minimum radiation efficiency of 97%.

REFERENCES

1. Sagne, D. and R. A. Pandhare, "Design and analysis of inscribed fractal super wideband antenna for microwave applications," *Progress In Electromagnetics Research C*, Vol. 121, 49–63, 2022.
2. Ali, T., B. K. Subhash, S. Pathan, and R. C. Biradar, "A compact decagonal-shaped UWB monopole planar antenna with truncated ground plane," *Microwave and Optical Technology Letters*, Vol. 60, No. 12, 2937–2944, 2018.
3. Azim, R., M. T. Islam, H. Arshad, M. M. Alam, N. Sobahi, and A. I. Khan, "CPW-fed superwideband antenna with modified vertical bow-tie-shaped patch for wireless sensor networks," *IEEE Access*, Vol. 9, 5343–5353, 2020.

4. Alluri, S. and N. Rangaswamy, "Compact high bandwidth dimension ratio steering-shaped super wideband antenna for future wireless communication applications," *Microwave and Optical Technology Letters*, Vol. 62, No. 12, 3985–3991, 2020.

5. Dey, S. and N. C. Karmakar, "Design of novel super wide band antenna close to the fundamental dimension limit theory," *Scientific Reports*, Vol. 10, No. 1, 16306, 2020.

6. Jamlos, M. A., M. F. Jamlos, S. Khatun, and A. H. Ismail, "A compact super wide band antenna with high gain for medical applications," *2014 IEEE Symposium on Wireless Technology and Applications (ISWTA)*, 106–109, IEEE, 2014.

7. Kundu, S. and A. Chatterjee, "A compact super wideband antenna with stable and improved radiation using super wideband frequency selective surface," *AEU — International Journal of Electronics and Communications*, Vol. 150, 154200, 2022.

8. Balani, W., M. Sarvagya, A. Samasgikar, T. Ali, and P. Kumar, "Design and analysis of super wideband antenna for microwave applications," *Sensors*, Vol. 21, No. 2, 477, 2021.

9. Dorostkar, M. A., M. T. Islam, and R. Azim, "Design of a novel super wide band circular-hexagonal fractal antenna," *Progress In Electromagnetics Research*, Vol. 139, 229–245, 2013.

10. Okan, T., "A compact octagonal-ring monopole antenna for super wideband applications," *Microwave and Optical Technology Letters*, Vol. 62, No. 3, 1237–1244, 2020.

11. Ramanujam, P., P. G. R. Venkatesan, C. Arumugam, and M. Ponnusamy, "Design of miniaturized super wideband printed monopole antenna operating from 0.7 to 18.5 GHz," *AEU — International Journal of Electronics and Communications*, Vol. 123, 153273, 2020.

12. Alluri, S. and N. Rangaswamy, "Compact high bandwidth dimension ratio steering-shaped super wideband antenna for future wireless communication applications," *Microwave and Optical Technology Letters*, Vol. 62, No. 12, 3985–3991, 2020.